Optical anisotropic metamaterials: Negative refraction and focusing

Anan Fang[1]**,Thomas Koschny**[1,2] **and Costas M. Soukoulis**[1,2,*]

[1] *Ames Laboratory and Department of Physics and Astronomy, Iowa State University, Ames, Iowa 50011, USA*

[2] *Institute of Electronic Structure and Laser, FORTH, and Department of Materials Science and Technology, University of Crete, 71110 Heraklion, Crete, Greece*

[*] *soukoulis@ameslab.gov*

Abstract: We design 3D metallic nanowire media with different structures and numerically demonstrate they can be effective homogeneous indefinite anisotropic media by showing their dispersion relations are hyperbolic. A nice fitting procedure is exploited to obtain the dispersion relations, from which we retrieve the effective permittivities. The pseudo focusing for the real 3D wire medium agrees very well with the homogeneous medium having the effective permittivity tensor of the wire medium. Studies also show that in the long wavelength limit, the hyperbolic dispersion relation of the 3D wire medium can be valid even for evanescent modes.

OCIS codes: (160.4760) Optical properties; (160.3918) Materials: Metamaterials

References and links

1. V. G. Veselago, "Electrodynamics of substances with simultaneously negative values of sigma and mu," Soviet Phys. Uspekhi-ussr **10**, 509–514 (1968).
2. J. B. Pendry, "Negative refraction makes a perfect lens," Phys. Rev. Lett. **85**, 3966–3969 (2000).
3. J. B. Pendry, D. Schurig, and D. R. Smith, "Controlling electromagnetic fields," Science **312**, 1780–1782 (2006).
4. M. Notomi, "Theory of light propagation in strongly modulated photonic crystals: Refractionlike behavior in the vicinity of the photonic band gap," Phys. Rev. B **62**, 10,696–10,705 (2000).
5. C. Y. Luo, S. G. Johnson, J. D. Joannopoulos, and J. B. Pendry, "Negative refraction without negative index in metallic photonic crystals," Optics Express **11**, 746–754 (2003).
6. E. Cubukcu, K. Aydin, E. Ozbay, S. Foteinopoulou, and C. M. Soukoulis, "Negative refraction by photonic crystals," Nature **423**, 604–605 (2003).
7. S. Foteinopoulou and C. M. Soukoulis, "Negative refraction and left-handed behavior in two-dimensional photonic crystals," Phys. Rev. B **67**, 235107 (2003); "Electromagnetic wave propagation in two-dimensional photonic crystals: A study of anomalous refractive effects," Phys. Rev. B **72**, 165112 (2005).
8. R. Moussa, S. Foteinopoulou, L. Zhang, G. Tuttle, K. Guven, E. Ozbay, and C. M. Soukoulis, "Negative refraction and superlens behavior in a two-dimensional photonic crystal," Phys. Rev. B **71**, 085106 (2005).
9. A. Berrier, M. Mulot, M. Swillo, M. Qiu, L. Thylen, A. Talneau, and S. Anand, "Negative refraction at infrared wavelengths in a two-dimensional photonic crystal," Phys. Rev. Lett. **93**, 073902 (2004).
10. E. Schonbrun, Q. Wu, W. Park, T. Yamashita, C. J. Summers, M. Abashin, and Y. Fainman, "Wave front evolution of negatively refracted waves in a photonic crystal," Appl. Phys. Lett. **90**, 041113 (2007).
11. X. H. Hu and C. T. Chan, "Photonic crystals with silver nanowires as a near-infrared superlens," Appl. Phys. Lett. **85**, 1520–1522 (2004).
12. D. R. Smith and D. Schurig, "Electromagnetic wave propagation in media with indefinite permittivity and permeability tensors," Phys. Rev. Lett. **90**, 077405 (2003).
13. D. R. Smith, D. Schurig, J. J. Mock, P. Kolinko, and P. Rye, "Partial focusing of radiation by a slab of indefinite media," Appl. Phys. Lett. **84**, 2244–2246 (2004).
14. A. J. Hoffman, L. Alekseyev, S. S. Howard, K. J. Franz, D. Wasserman, V. A. Podolskiy, E. E. Narimanov, D. L. Sivco, and C. Gmachl, "Negative refraction in semiconductor metamaterials," Nature Materials **6**, 946–950 (2007).

15. R. Wangberg, J. Elser, E. E. Narimanov, and V. A. Podolskiy, "Nonmagnetic nanocomposites for optical and infrared negative-refractive-index media," J. Opt. Soc. Am. B-optical Phys. **23**, 498–505 (2006).
16. J. Yao, Z. W. Liu, Y. M. Liu, Y. Wang, C. Sun, G. Bartal, A. M. Stacy, and X. Zhang, "Optical negative refraction in bulk metamaterials of nanowires," Science **321**, 930–930 (2008).
17. I. V. Lindell, S. A. Tretyakov, K. I. Nikoskinen, and S. Ilvonen, "BW media-media with negative parameters, capable of supporting backward waves," Microwave Opt. Technology Lett. **31**, 129–133 (2001).
18. M. Scalora, G. D'Aguanno, N. Mattiucci, M. J. Bloemer, D. de Ceglia, M. Centini, A. Mandatori, C. Sibilia, N. Akozbek, M. G. Cappeddu, M. Fowler, and J. W. Haus, "Negative refraction and sub-wavelength focusing in the visible range using transparent metallodielectric stacks," Optics Express **15**, 508–523 (2007).
19. B. Wood, J. B. Pendry, and D. P. Tsai, "Directed subwavelength imaging using a layered metal-dielectric system," Phys. Rev. B **74**, 115116 (2006).
20. Z. Jacob, L. V. Alekseyev, and E. Narimanov, "Optical hyperlens: Far-field imaging beyond the diffraction limit," Optics Express **14**, 8247–8256 (2006).
21. Y. Liu, G. Bartal, and X. Zhang, "All-angle negative refraction and imaging in a bulk medium made of metallic nanowires in the visible region," Opt. Express **16**, 15,439–15,448 (2008).
22. E. D. Palik and G. Ghosh, *The electronic handbook of optical constants of solids* (Academic Press, 1999).
23. J. Elser, R. Wangberg, V. A. Podolskiy, and E. E. Narimanov, "Nanowire metamaterials with extreme optical anisotropy," Appl. Phys. Lett. **89**, 261102 (2006).
24. A. Sihvola, *Electromagnetic Mixing Formulas and Applications* (Institution of Electrical Engineers, 1999).
25. C. A. Foss, G. L. Hornyak, J. A. Stockert, and C. R. Martin, "Template-synthesized nanoscopic gold particles - optical-spectra and the effects of particle-size and shape," J. Phys. Chem. **98**, 2963–2971 (1994).

1. Introduction

Recently negative index materials (NIMs) and photonic crystals (PCs) are getting more and more attention because of its extraordinary optical properties like near field focusing, subwavelength imaging, and negative refraction [1-11]. As first proposed, these NIMs have the permittivity ε and the permeability μ simultaneously negative, which are achieved by overlapping electric and magnetic resonances. But the double resonance scheme also causes large resonance losses and technical difficulties in design and fabrication. In addition to negative index materials, both theoretical and experimental studies show that the properties of negative refraction and subwavelength imaging can also occur in some uniaxially anisotropic media, which can have lower losses and be easier to fabricate [12-21]. For a particular anisotropic medium, where the permittivity component ($\varepsilon_\perp$) along the direction perpendicular to the interface is negative while all other permittivity and permeability components are positive, it has a hyperbolic dispersion relation as follows:

$$\frac{k_\perp^2}{|\varepsilon_\parallel|\,\mu} - \frac{k_\parallel^2}{|\varepsilon_\perp|\,\mu} = \omega^2 \tag{1}$$

where the definitions for $\varepsilon_\perp$, $\varepsilon_\parallel$, $k_\perp$ and $k_\parallel$ are shown in Fig. 1(b). Fig. 1(a) schematically shows how negative refraction works in this particular medium. The group velocity can be calculated by $\mathbf{v}_g = \nabla_{\mathbf{k}}\omega(\mathbf{k})$, which specifies the direction of group velocity (energy flow) would be normal to the equifrequency surface (EFS) and in the direction where ω is increasing. The conservation of $k_\parallel$ indicates two possible solutions in the medium, but the correct one can be determined by casuality - the refracted group velocity should point away from the interface, as shown in Fig. 1(a). From this figure, we can see that for isotropic medium, the circular equifrequency surface forces the the refracted phase and group velocities to lie in the same line - antiparallel for negative index medium while parallel for positive index medium. For anisotropic medium with hyperbolic dispersion relation, they do not lie in the same line any more except for the case when $k_\parallel = 0$. To be normal to the hyperbolic curves and satisfy the requirement of pointing away from the interface coming from the casuality, the refracted group velocity have to undergo a negative refraction , which causes our expected focusing. (Note: the refracted phase velocity for anisotropic medium still has a positive refraction.)

In this paper, we numerically demonstrate that this particular anisotropic material can be

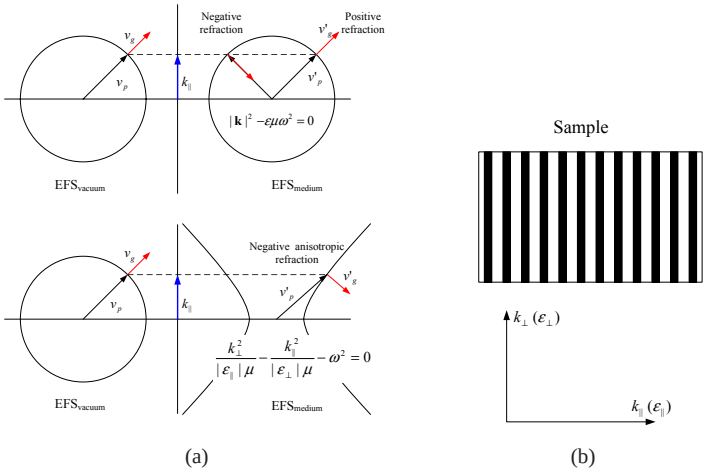

Fig. 1: (a) Top graph: Circular equifrequency surfaces (EFS) for vacuum and isotropic media. Bottom graph: equifrequency surfaces for vacuum (circle) and negative anisotropic refraction medium (hyperbolic relation). The incident phase velocity direction is indicated by black arrow, which is parallel to the incident group velocity (red arrow) in vacuum. The refracted phase velocity (black arrow) and group velocity (red arrow) in isotropic positive medium are parallel to each other, while they are antiparallel in isotropic negative medium. In negative anisotropic refraction medium, the directions of phase velocity and group velocity are not fixed. The wave vector component $k_\parallel$ (blue arrow) parallel to interface is conserved. (b) The definitions for $k_\perp$, $k_\parallel$, $\varepsilon_\perp$ and $\varepsilon_\parallel$ used in our simulations.

realized by a 3D wire medium that can operate in optical region. Its numerically obtained dispersion relation shows the existence of a hyperbolic relation in the long wavelength limit and then gives the effective permittivity of the 3D wire medium. The imaging for a homogeneous slab with the effective permittivity shows a very good agreement with the real 3D wire medium. All simulations about this effective homogeneous anisotropic medium are done by comsol multiphysics, an electromagnetic solver based on finite element method (FEM).

2. Superlattice of metallic-air layers

Before discussing our results of 3D wire medium, simulations are performed for a superlattice of metallic layers with $\varepsilon = -4$ and air layers with $\varepsilon = 1$ as shown in Fig. 1(b). These simulations are done to check the applicability of our idea that one can obtain negative refraction and focusing in anisotropic media. Our simulation results show that there exist the negative refraction in Fig. 2(a) and pseudo-focusing in Fig. 2(c). The focusing simulation is compared with the ray-tracing diagram (Fig. 2(b)) and the imaging of a homogeneous anisotropic slab with the effective permittivity extracted from the dispersion relation of the metallic-air superlattice (Fig. 2(d)). The effective parameters for $\varepsilon_\parallel$ and $\varepsilon_\perp$ are obtained by extracting $\mathbf{k}$ from the field distribution of a plane wave incidence inside the slab and then fitting with the hyperbolic dispersion given by Equation [1]. The details of obtaining the effective parameters $\varepsilon_\parallel$ and $\varepsilon_\perp$ will be dicussed below. One can see the pseudo focusing for the real metallic-air superlattice agrees very well with the homogeneous medium.

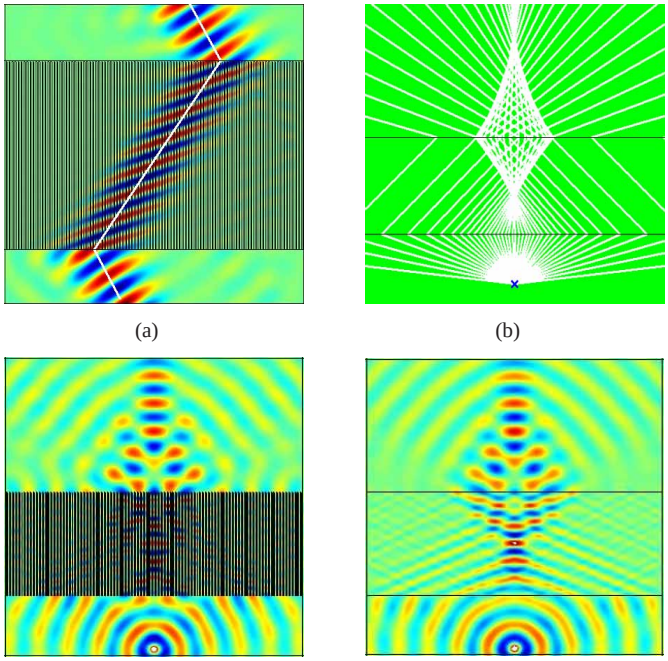

(a) (b)

(c) (d)

Fig. 2: Material parameters of the metallic layers: $\varepsilon = -4$, $\mu = \mu_0$; Working frequency: $f =$ 0.5 GHz; Space period of metallic layers: 0.06 m; Width of metallic layers: 0.02 m. (a) The magnetic field distribution of the group negative refraction in the metallic-air layers array slab. A gaussian beam with transverse magnetic polarization and an incident angle of 30^0 is incident on the simulated metallic-air superlattice. The white line indicates the ray tracing result. (b) A ray-tracing diagram showing the rays coming out from a line source are refocused by an anisotropic medium slab with the effective permittivity ε tensor of our simulated metallic-air layers array slab. (c) The magnetic field distribution of pseudo focusing of our simulated metallic plates array slab with a line source placed 1.25 m from the interface, which launches a cylindrical transverse magnetic polarized wave. The thickness and the width of metallic-air layers array slab are 2.4 m and 6 m, respectively. (d) The magnetic field distribution of pseudo focusing in the a homogeneous anisotropic slab with the effective permittivity of our simulated metallic-air layers array slab ($\varepsilon_{\|} = 1.7293,\ \varepsilon_{\perp} = -0.7907$).

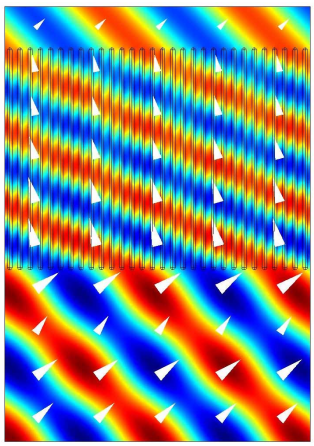

Fig. 3: The magnetic field distribution for negative refraction in a 3D gold-wire square lattice medium with vacuum background and the wavelength $\lambda = 700$ nm. The incident plane wave has transverse magnetic polarization and an incident angle of 45^0. The permittivity ε for gold is taken from experimental data [22]: $\varepsilon = -15.5931 + i\ 1.2734$ at $\lambda = 700$ nm. The radii, length of gold wire and the lattice constant are 16 nm, 1532 nm and 70 nm, respectively. The white arrow indicates the direction of power flow.

3. Obtain numerical dispersion relations

To check if the wire medium constitues our desired effective anisotropic homogeneous medium, it is straightforward to obtain its numerical dispersion relation first. On this purpose, we exploit a fitting procedure to extract **k** from the phase propagation. In the long wavelength limit, electromagnetic metamaterials should behave like a homogeneous medium. When a plane wave incidents on a homogeneous slab with an incident angle θ_i, forms a stationary wave inside the slab instead of a travelling wave because of the reflections in the two interfaces. Since $k_\perp$ represents the field variation in the perpendicular direction, we can take a cross section along this direction and analytically obtain the field distribution in the cross section by considering the multireflections inside the slab as follows:

$$F(y) = A\frac{e^{-\alpha(y-y_0)}e^{i[k_\perp(y-y_0)+\theta]} + re^{\alpha(y-y_0-2d)}e^{-i[k_\perp(y-y_0-2d)-\theta]}}{1-r^2e^{-2\alpha d}e^{2ik_\perp d}} \tag{2}$$

Where y is the position in the perpendicular direction within the cross section, $F(y)$ is the field at the position y, A and θ are the field amplitude and the field phase at the starting point of the cross section in the perpendicular direction $y = y_0$ (i.e., the location of the first interface of the slab), α is the decaying factor of the homogeneous slab, $k_\perp$ is the perpendicular component of the wave vector **k**, d is the thickness of the slab and r is the reflection coefficient in the two interfaces.

By fitting the numerically obtained field distribution along the perpendicular direction in a cross section with the theoretical formulas above, we can obtain the $k_\perp$ inside the wire medium slab for an incident plane wave with an incident angle θ_i. For $k_\parallel$, we can easily get $k_\parallel = k_0 sin\theta_i$ from the incident angle θ_i since $k_\parallel$ is conserved across the interfaces,where k_0 is the wavevector in the background. Consequently, we can have the numerical dispersion relation of the wire medium by getting $k_\parallel$ and $k_\perp$ for different incident angles.

4. 3D anisotropic wire medium

The first structure for the 3D anisotropic wire medium in the optical region is a 3D gold-wire square lattice with the wire radius $r = 16$ nm and the lattice constant $a = 70$ nm in vacuum. Fig. 3 shows that the group negative refraction occurs when a plane wave with the wavelength $\lambda = 700$ nm and transverse magnetic polarization incidents on our simulated slab with an incident angle of 45^0, while the phase velocity still undergoes a positive refraction. Pseudo focusing

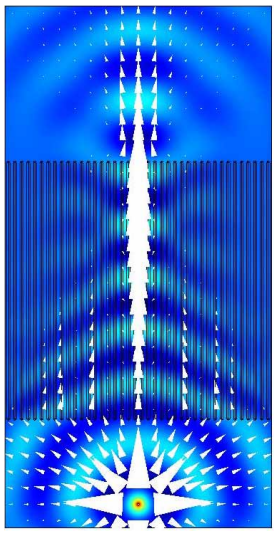

Fig. 4: The magnetic field distribution of pseudo focusing in a 3D gold-wire square lattice medium with a line source placed 884 nm away from the interface, which launches a cylindrical transverse magnetic polarization wave at wavelength $\lambda = 700$ nm. The permittivity of gold is the same as in Fig.3. The background is vacuum. The radii, length of gold wire and the lattice constant are 16 nm, 2732 nm and 70 nm, respectively. The white arrow indicates the direction of power flow.

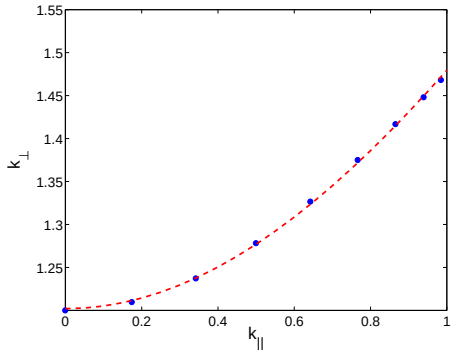

Fig. 5: The numerical dispersion relation data from simulation (solid circles) and the fitted hyperbolic curve (dashed line). All parameters are the same as in Fig 4 except the length of gold wire is 1500 nm. Note: all k components here are normalized by k_0, where $k_0 = \omega/c$.

can also be seen from Fig. 4 , where the transverse magnetic polarized wave with wavelength $\lambda = 700$ nm coming out from a line source is focused inside the simulated slab, then refocused on the other side of the slab.

When the geometric parameters, the wire radius $r = 16$ nm and the lattice constant $a = 70$ nm, are much smaller than the vacuum wavelength $\lambda = 700$ nm of the incident EM wave, the 3D wire medium can be considered as an effective medium [23-25]. The numerical dispersion relation of this 3D gold-wire square lattice medium is obtained and shown in Fig. 5. The effective permittivity $\varepsilon_\perp = -1.9082 + i\ 0.2391$ and $\varepsilon_\parallel = 1.4455 + i\ 0.0044$ are obtained by fitting the numerical dispersion data into the hyperbolic dispersion relation (Equation [1]). The fitted curve (dashed line) shows the fitting is pretty good and the simulated metamaterial does have a hyperbolic dispersion relation.

We also have used the Maxwell-Garnett equations [24, 25] to obtain the effective $\varepsilon_\perp$ and $\varepsilon_\parallel$ at $\lambda = 700$ nm for different filling ratios for the square lattice of metallic wires. In Fig. 6, we present the fitted results for $\varepsilon_\parallel$ and $\varepsilon_\perp$ for different radii, while keeping the lattice constant unchanged. We use the following expressions for $\varepsilon_\parallel$ and $\varepsilon_\perp$ from the Maxwell-Garnett theory:

$$\varepsilon_\parallel = \varepsilon_d \left[\frac{(1+f)\varepsilon_m + (1-f)\varepsilon_d}{(1-f)\varepsilon_m + (1+f)\varepsilon_d} \right] \tag{3}$$

$$\varepsilon_\perp = f\varepsilon_m + (1-f)\varepsilon_d \tag{4}$$

Fig. 6: The effective permittivity $\varepsilon_\perp$ and $\varepsilon_\parallel$ calculated from Maxwell-Garnett equations (solid lines) and numerical simulations (squares) for different wire radius. The simulated medium is a 3D square lattice silver wire medium in vacuum with lattice constant $a = 20$ nm. The wavelength is $\lambda = 700$ nm. The permittivity of silver at $\lambda = 700$ nm is $\varepsilon_{silver} = -20.4373 + i\ 1.2863$, taken from experimental data [22] .

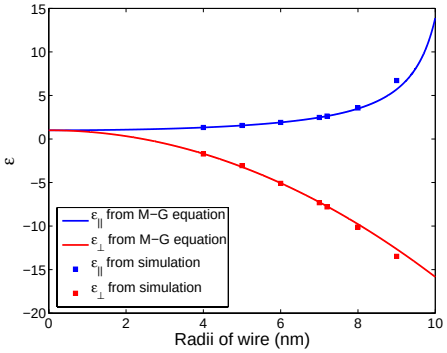

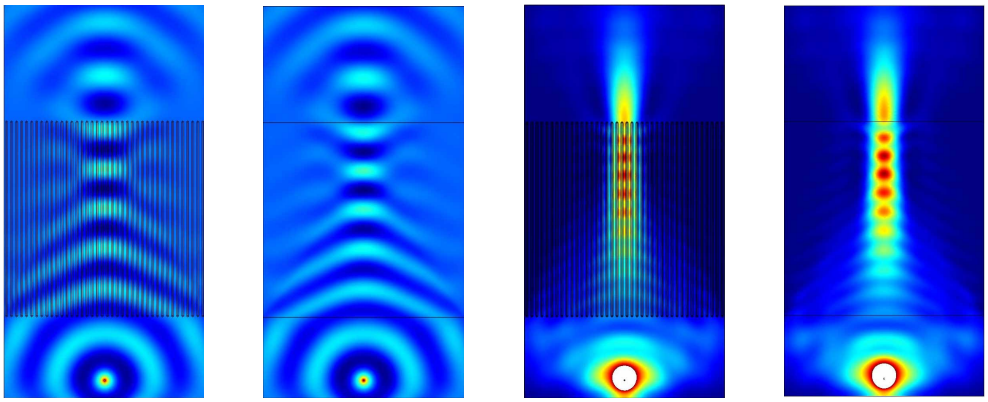

(a) (b) (c) (d)

Fig. 7: (a) The magnetic field distribution of focusing simulation for the simulated 3D gold-wire square lattice anisotropic medium slab. (b) same as (a), but for a homogeneous anisotropic slab with the fitted effective permittivity $\varepsilon_\parallel = 1.4455 + i\ 0.0044$ and $\varepsilon_\perp = -1.9082 + i\ 0.2391$. (c) and (d) are same as (a) and (b), respectively, but for the magnetic field intensity distribution. All material parameters are the same as in Fig.4.

where f is the filling ratio of the metal, ε_m and ε_d are the permittivity of metal and dielectric, respectively. Notice that the effective values of $\varepsilon_\perp$ and $\varepsilon_\parallel$ agree reasonably well with our fitting procedure. This is due to the effect that the vacuum wavelength $\lambda = 700$ nm is much larger than the lattice constant and the radius of the metallic wires. In other cases, the effective parameters given by Eqns. [3] and [4] do not agree with our fitting procedure.

For comparison, we replace this 3D gold-wire square lattice medium slab with a homogeneous anisotropic slab with the fitted effective permittivity $\varepsilon_\parallel = 1.4455 + i\ 0.0044$ and $\varepsilon_\perp = -1.9082 + i\ 0.2391$ (All other parameters are the same, such as thickness and width of the slab, source and distance between the source and the first interface, etc.). The simulation results for magnetic field distribution and magnetic field intensity are shown in Fig. 7. One can see that both of them have very good agreements between the homogeneous slab and the 3D wire medium . The excellent agreement proves again that our simulated 3D gold-wire square lattice metamaterial has a hyperbolic dispersion relation and our fitting procedure works very well.

To be experimentally feasible, the second structure we examine is a hexagonal lattice struc-

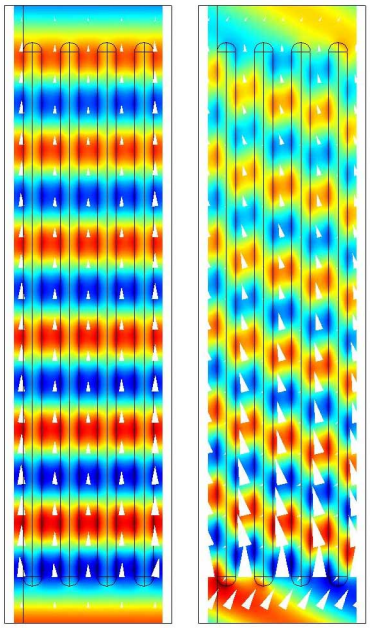

(a) (b)

Fig. 8: The magnetic field distribution in a 3D silver-wire hexagonal lattice medium slab with alumina background. The incident plane wave has transverse magnetic polarization and wavelength in vacuum $\lambda = 700$ nm. (a) normal incidence (b) at an incident angle of 30^0. The white arrow indicates the direction of power flow. The hexagonal lattice constant a, the radius r and the length l of silver wires are 120 nm, 30 nm and 1700 nm, respectively. The permittivities of silver and alumina at wavelength in vacuum $\lambda = 700$ nm are $\varepsilon_{silver} = -20.4373 + i\ 1.2863$ and $\varepsilon_{Al_2O_3} = 3.1$, respectively, taken from experimental data [22].

ture composed of silver wires in alumina background. Fig. 8 shows the magnetic field distributions along a cross section perpendicular to the magnetic field for two different incident angles (0^0 and 30^0). For the incident angle θ=30^0 case (Fig. 8(b)), one can see that the group velocity (white arrow) undergoes a negative refraction inside the simulated medium. A substantial decay in the perpendicular direction for the magnetic field and the power flow exists for both of these two different incident angles (Fig. 8(a) and Fig. 8(b)), since the lossy metallic wires have a very high filling ratio in this particular wire medium.

By the same fitting procedure, the numerical dispersion relation for the 3D silver-wire hexagonal lattice medium can also be obtained and is shown in Fig. 9(a). The lowest 4 points are used to fit with a hyperbolic dispersion curve and the effective permittivities are $\varepsilon_{\|} = 5.3653 + i\ 0.0708$ and $\varepsilon_{\perp} = -2.9188 + i\ 0.4571$. One can see that the large $k_{\|}$ points deviate from the fitted curve, even though the lowest 4 points are fitted very well. That's because we have a small wavelength/spatial period ratio around 3.3 in alumina, which causes the breakdown of the homogeneous effective medium approximation in large $k_{\|}$ region.

To extend the "good fitted" region to a larger $k_{\|}$ range where the numerical dispersion points can fit well into a hyperbolic dispersion curve, we reduce the hexagonal lattice constant and the radius of silver wires to a smaller value $a = 30$ nm and $r = 12$ nm, respectively, while keeping all other parameters the same as before, so that we can have a much higher wavelength/spatial period ratio around 13. The fitted numerical dispersion relation is shown in Fig. 9(b). The lowest 10 points, which are propagating modes (i.e., $k_{\|} \leq k_0$, where $k_0 = \sqrt{\varepsilon}\omega/c$ and ε is the permittivity of alumina.), are used to fit with a hyperbolic dispersion curve. The obtained effective permittivities are $\varepsilon_{\|} = 22.1505 + i\ 1.4693$ and $\varepsilon_{\perp} = -13.7714 + i\ 0.6882$. If we use Eqns [3] and [4], the Maxwell-Garnett effective permittivities are given by $\varepsilon_{\|} = 25.8371 + i\ 2.0791$ and $\varepsilon_{\perp} = -10.5614 + i\ 0.7466$, which does not agree well with our fitting parameters. In Fig. 9(b), one can see that the numerical dispersion relation data from our fitting procedure are fitted very well into a hyperbolic dispersion curve, even for those large $k_{\|}$ points where

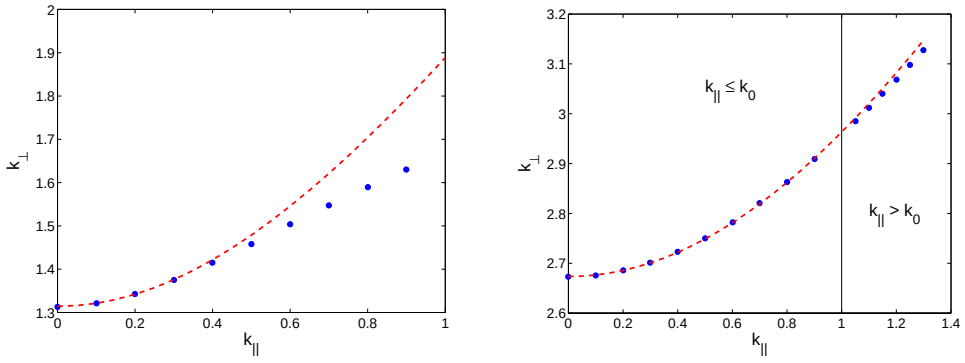

(a) (b)

Fig. 9: The numerical dispersion (solid circles) and the fitted dispersion curve (dashed line) of 3D silver-wire hexagonal lattice media in alumina background. (a) lattice constant $a = 120$ nm and radii of silver wire $r = 30$ nm. (b) lattice constant $a = 30$ nm and radii of silver wire $r = 12$ nm. $k_{\|} \leq k_0$ corresponds to the propagating modes in background, while $k_{\|} > k_0$ corresponds to evanescent modes. All other parameters are the same as in Fig 7. Note: all k components are normalized by k_0, where $k_0 = \sqrt{\varepsilon}\omega/c$ and ε is the permittivity of alumina.

$k_{\|} > k_0$, which are evanescent modes and essential for super-resolution applications.

5. Conclusion

We present two anisotropic metamaterials that demonstrate negative refraction and focusing. The first system is a superlattice of metal-dielectric structure and the second system is a three-dimensional (3D) metallic wires embedded in a dielectric matrix. We first obtain the numerical dispersion relation for the two cases by simulating the eigenmodes of the realistic system. The hyperbolic dispersion relation is obeyed in both of the two cases, where the effective permittivities have opposite signs in the two propagation directions. Our simulations of the realistic structures, as well as the homogeneous simulations show negative refraction for all incident angles and demonstrate focusing. The metallic nanowires can be valid for evanescent modes in the dielectric background by having a large wavelength/spatial period ratio, which has important applications in super-resolution.

In conclusion, we numerically demonstrate that an effective homogeneous indefinite anisotropic medium can be realized by a 3D nanowire medium at optical frequency region, which can have a negative refraction and pseudo focusing. We also present a nice fitting procedure by which we can obtain the numerical dispersion relation of our 3D wire medium and then retrieve its effective permittivity. Meanwhile, we demonstrate that the hyperbolic dispersion relation of the 3D nanowire medium can be valid for evanescent modes in background by having a large wavelength/spatial period ratio (i.e., in the long wavelength limit), which may have important applications in super-resolution.

6. Acknowledgement

Work at Ames Laboraory was supported by the Department of Energy (Basic Energy Science) under Contract NO. DE-ACD2-07CH11358. This work was partially suported by AFOSR under MURI grant (FA 9550-06-1-0337) and the European Community project ENSEMBLE.